Interaction of small gas phase molecules with alumina supported rhodium nanoparticles: an *in situ* spectroscopic study

2008 J. Phys.: Condens. Matter 20 184020

(http://iopscience.iop.org/0953-8984/20/18/184020)

IOP PUBLISHING JOURNAL OF PHYSICS: CONDENSED MATTER

J. Phys.: Condens. Matter **20** (2008) 184020 (10pp) doi:10.1088/0953-8984/20/18/184020

Interaction of small gas phase molecules with alumina supported rhodium nanoparticles: an *in situ* spectroscopic study

J Evans and M Tromp

School of Chemistry, University of Southampton, Southampton SO17 1BJ, UK

E-mail: je@soton.ac.uk and M.Tromp@soton.ac.uk

Received 28 November 2007
Published 17 April 2008
Online at stacks.iop.org/JPhysCM/20/184020

Abstract

Supported nanoparticulate Rh systems are studied as a model system for the important three way catalysts as used in the combustion engines of cars. Small Rh nanoparticles with a small particle size distribution can be easily synthesized and their morphology is studied using x-ray absorption fine structure (XAFS) spectroscopy. The interaction of the supported rhodium nanoparticles on γ-Al_2O_3 with small gas phase molecules like H_2, O_2, CO, NO, H_2S and SO_2 is investigated, *in situ* and time resolved, using a combination of techniques, i.e. XAFS, diffuse reflectance infrared Fourier transform spectroscopy (DRIFTS) and mass spectrometry. The surface species formed upon exposure of the metal particles to the adsorbing molecules, and their sometimes disruptive interaction with the metal particles, are identified as a function of temperature and time. Dynamic equilibria are observed which change the oxidation state and the nuclearity of the supported rhodium particles under operational conditions. Rather than merely adsorb on a catalyst particle, these gases have a substantial role in defining the nature of the particle.

(Some figures in this article are in colour only in the electronic version)

1. Introduction

Nanoscale metal particles provide the basis of an important class of catalysts. They provide an ensemble of metal atoms with vacant coordination sites that may be adept at binding molecules (chemisorption), dissociating them (dissociative chemisorption) and recombining them in a rearranged manner. Once these products leave the particle, it is restored to its original form. Thus the metal particle will have mediated the chemical transformation without any net alteration, and so conforms to the Berzelius definition of a catalyst [1, 2]. The ideal particle size will be the smallest one necessary to effect the catalysis efficiently. Significantly larger particles will have a lower surface/bulk ratio and sequester a proportion of metal atoms in inaccessible sites.

The aims of catalyst synthesis are often rather different from those behind surface science studies, where crystallographic order of surface and adsorbates may be achieved [2, 3]. Generally supported metal catalysts have metallic particles chemisorbed onto the surface of an inert, or a promoting solid, such as a high surface area oxide or carbon. This will maximize the density of the active sites in a manner which may restrict their aggregation, or sintering. The high area of the support means that the packing density of active sites in a reactor can be maximized. The high specific area is achieved either by having a very small particle size or by having a porous solid with a high internal surface area, there being four classifications.

(1) High areas and high order can be married in some microporous solids, such as zeolites and zeotypes (e.g. aluminium phosphate (AlPO) materials). But generally the pore size (<1 nm) restricts both the size of the metal particle and also the pathways for access of the reagents, the extraction of products and the conformations of the adsorbates.
(2) Mesoporous oxides can provide a degree of order on the nm length scale and provide a greater pore diameter

thus allowing larger particle sizes (<10 nm). The mesoscopic order provides an approximately uniform set of pore diameters but the surface sites within the pores are non-uniform and disordered.

(3) Macroporous oxides, generally formed as gels by precipitation from solution, are even less ordered, and possess a distribution of pore sizes.

(4) Non-porous supports can only achieve a high specific area by having a very small particle sizes (10–20 nm); these are often formed by vapour phase hydrolysis or oxidation. While some such materials present single crystal planes, as in MgO smoke which contains cubes with (100) faces, the majority have very low surface crystallinity, even if there is an underlying crystalline bulk [4, 5].

To add to the structural complexity, the control of particle size and shape by chemical reduction of metal salts or complexes is imperfect; a distribution of particle morphologies results, each with a spectrum of reactive sites and located on a particular topography of the support. So structure–function correlations can be elusive. Catalytic reactions may be divided between structure sensitive (requiring a specific local ensemble of metal atoms) and structure insensitive (where a variety of sites can mediate the transformation, or possibly where sites are in rapid dynamic equilibrium). The former only should be expected to show a catalytic performance which is a function of particle size, but often these correlations are inconsistent [6].

Attempting to unravel this complexity inevitably requires some simplification, and the two extremes are (i) the molecular approach of organometallic chemistry, starting from mononuclear metal complexes to nuclearities of a few 10s of metal atoms [5, 7], and (ii) the surface science model of identifying the chemistry on particular crystal planes of known structure [2]. Correlations between these approaches (cluster–surface analogy) have been productive in providing a data bank of characteristic spectral features for identifying surface bound species [7].

In any case, establishing the validity of a particular approach does require a direct structural description of the metal catalyst. In addition it is important to establish the sensitivity of the structures to differing conditions of temperature and of the concentrations of the reagents. The low degree of structural order in these catalysts limits the efficacy of x-ray diffraction methods. Instead x-ray absorption spectroscopy may be employed as the core technique for a structural assessment of nanoparticulate catalysts under reaction conditions. It provides a partial radial distribution function around the adsorbing atom, in any phase. In principle, by choosing to study the absorption edges of the metals within the active particles, those of the supports, and those of adsorbates and poisons, a series of mean local structures may be derived. This is still an incomplete and averaged structural description, and evidence should be accrued from a combination of techniques to try to eliminate some structural models. Here we relate direct structure–function studies aimed at unravelling some of these complexities. Only the absorption edge of the metal was utilized, the other edges being too low in energy to allow *in situ* studies. Accordingly IR and mass spectrometry were employed to monitor the adsorbates.

The aims of this work are very similar to studies of adsorption on ordered single crystal surfaces: namely to establish the molecular level correlation between structure and reactivity related to surface catalysis. The experimental approach is substantially modified due to the different physical nature and chemical complexity of these samples which are more akin to operating catalysts.

2. X-ray absorption fine structure (XAFS) of supported metal catalysts

2.1. Appropriateness of XAFS for probing nanoparticulate metals

The absorption of an x-ray photon can cause a core-valence transition which contributes to the x-ray absorption near edge structure (XANES). The shape and energy of these features are influenced by the local charge and structure at the absorbing atom. If the photon has energy in excess of this, allowing promotion to the continuum, then a photoelectron wave results. The back scattering by the potentials of neighbouring atoms creates an interference effect (extended x-ray absorption fine structure, EXAFS) thus affording a partial radial distribution which may be analyzed to identify the type of near-neighbour and to refine the number of these atoms and their interatomic distances from the absorbing atom.

This local effect is highly appropriate to study the predominantly amorphous supported metal catalysts. The energy of the absorption edge is dependent upon the atomic number of the element, and thus the partial radial distribution function (rdf) from the metal absorption edge will be selective for atoms in the supported particles without any interference from rdfs within the support. The absorption edges of most metals of interest (transition elements) are of sufficiently high energy to provide an acceptable penetration depth through the sample, reacting gases and cell walls or windows. Hence, *in situ* structural studies during catalytic processes are experimentally feasible using current synchrotron storage rings as the light source [8, 9], providing insights into the catalytic activity and selectivity as a function of reactant concentration and temperature.

Spectroscopic experiments under selected conditions do provide direct structural information about the metal in a relevant environment, however only in that equilibrium steady state of the nanoparticles. So there is little further insight into reaction mechanisms. This can be addressed by perturbing the reaction conditions by pulsing the reagents or carrying out temperature or pressure jumps to displace the system from equilibrium. Spectra should then be acquired rapidly enough to track the structures during the restoration of equilibrium to probe the kinetics of the structure changes and identify any transient species. The two XAFS methods to achieve this are QEXAFS (Quick EXAFS), in which the crystal monochromator is rotated rapidly to provide a rapid scan time (acquisition time of seconds) [10], or energy dispersive EXAFS (EDE), or DEXAFS (Dynamic EXAFS) [11], in which a curved crystal polychromator is utilize to provide the band of energies of the XAFS spectrum

simultaneously (milliseconds). Both approaches have provided valuable insights into heterogeneous catalysts [12, 13]. To enhance the partial structural information provided by XAFS, the simultaneous monitoring by other techniques with intrinsic chemical speciation (IR [14], Raman [15, 16], UV–visible [15, 17], XRD [18]) provides much additional insight.

2.2. Structural sensitivity to particle nuclearity

Both XANES and EXAFS are a function of the metal particle size and morphology, but they may be described in a different manner. The former will be affected by the density of empty states, with the orbitals probed in a dipole allowed transition being particularly important i.e. the empty states with p character at the K (1s) absorption edges and with d character at L_{III} (2p) edges. These densities of states are sensitive to particle size, since the ratio of surface/bulk atoms decreases with increasing nuclearity. In calculations on fcc rhodium particles very clear changes are observable at the Rh K-edge XANES region from 1 through to 19 metal atoms; convergence to the bulk structure was evident at a 55 atoms cluster [19, 20].

Although derived from the same x-ray absorption spectrum, the factors contributing to the EXAFS region do have a different emphasis. In an ordered metallic structure the first directly bonded distance to the neighbouring atoms dominates the backscattering pattern, but, as for XANES, contributions for the non-bonded distances are also very significant. In a close packed structure, the first shell coordination number varies from 1 for a dimer to 12 for an infinite slab. There is a strong curvature in this relationship [21]. At the same time, the precision of the coordination number is not very high (±10%) due to its direct correlation with other parameters like the Debye–Waller factor and inelastic effects [22]. The sensitivity to the coordination number becomes especially strongly attenuated above 100 atoms. The non-bonded distances can be used to differentiate the lattice type and have a higher sensitivity to particle size [23] and morphology [24]. To be able to derive accurate coordination numbers for these higher shells, the data needs to be of sufficiently high quality but this becomes increasing difficult due to the $1/r^2$ reduction in the density of the photoelectron wave (with $r = M \cdots M$ distance), the increase in Debye Waller factor and inelastic scattering. Moreover, the asymmetric pair distributions that occur in nanoparticulate catalysts can lead to a distortion of the real coordination number [25].

2.3. Instrumentation for in situ studies

The aim of these experiments was to establish a method that would rapidly follow structural changes as the temperature or gas composition above a catalyst was perturbed. Initial developments were performed on Station 9.3 at the SRS (Daresbury, UK) using the energy dispersive mode [26]. The characteristics of this optical arrangement are:

- there is a focal spot at the sample position which reduces the sample volume and thus reduces the associated gas volume;
- all spectral points are measured simultaneously, otherwise the acquisition time for a spectrum should be much shorter than the true time resolution of the experiment so that the entire spectrum is representative of the same population of species;
- the parallel acquisition allows acquisition times to be reduced to milliseconds.

The set-up and time resolution of the technique matches other multiplexed techniques such as UV–visible spectroscopy using a diode array [17] and rapid scanning Fourier transform IR [14]. At the same time, EDE is very demanding upon beam stability, the quality of optical components, and detector characteristics. There are also restrictions on the sample, like a high degree of homogeneity and to be measurable in a transmission, rather than a fluorescence (or electron yield) mode.

The initial study at the SRS showed that spectra could be recorded with a 50 ms time resolution for a 5 wt% platinum on silica sample at the Pt L_{III} edge (11.56 keV), but averaging over 100 spectra was necessary to achieve analyzable EXAFS data [27]. At a third generation storage ring, the ESRF (Grenoble, France), the undulator source on the dispersive beam line (ID24) provides a much higher x-ray flux at the sample, and the higher electron energy extends the viable x-ray energy to over 20 keV. This experimental station provides an excellent platform for time-resolved studies at the Rh (23.22 keV) and Pd (24.45 keV) K-edges. Exposure times for single spectra for 5 wt% Rh/Al_2O_3 are in the region of 2–4 ms [28], averaging of spectra still permitting synchronization with an IR spectrometer operating with a scan time of 60–100 ms [14, 29].

Measurements at the Rh K-edge have been carried out initially using a quartz cell microreactor [30] and more recently using a diffuse reflectance infrared Fourier transform spectroscopy (DRIFTS) cell [14, 29]. Here the sample rests as a powder in a boron nitride cup. The IR is probed from the surface of the catalyst bed, while the x-ray beam aligned just underneath the bed surface, so the XAFS measurement is effected on a region also studied by IR spectroscopy. For IR spectroscopy the DRIFTS geometry is more demanding than a transmission mode, but it obviates the need for the use of a pressed disc. That more common sampling method introduces interparticle voids, and the act of pressing the disc can cause local heating and metal particle fusing.

The sampling system is within a small environmental chamber with the gas composition monitored by multiple ion mass spectrometry, and the gas introduction controlled by mass flow controllers and gas switching valves. Up to 2004, detection was via a Princeton CCD camera, but the readout time for that unit of ∼300 ms was the main restriction in the measurement repetition rate. The FReLoN camera developed at the ESRF [31] removed that restriction with a readout time of ∼1.6 ms [28]. Presently the decrease in spectral acquisition and repeat time means that the limit of the time resolution of the experiment is the width of the gas pulse (∼1–3 s).

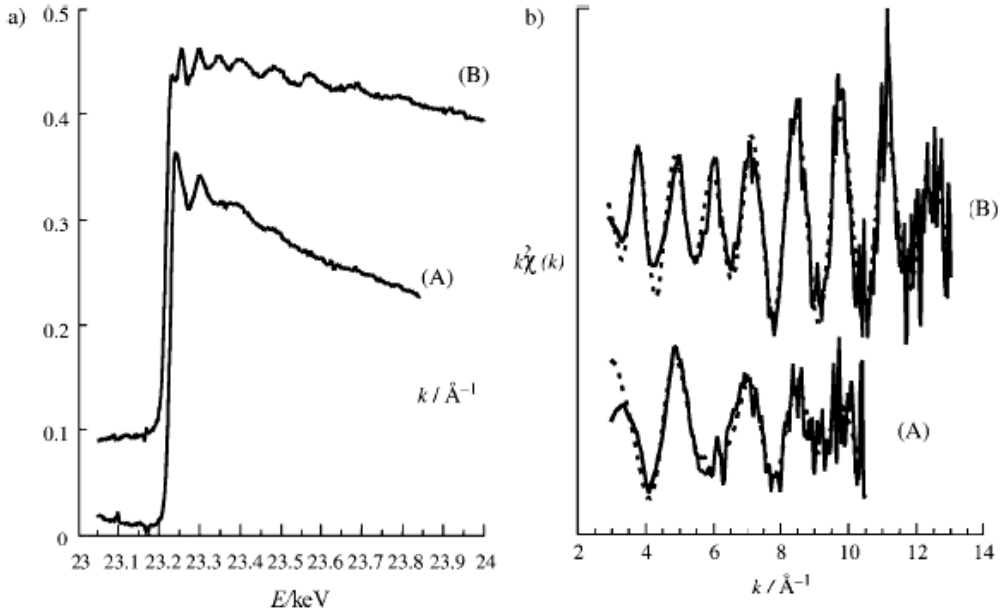

Figure 1. (a) Rh K-edge EDE spectra and (b) the extracted and fitted EXAFS data of 5 wt% Rh/Al_2O_3 of a 'fresh' catalyst (A) and one reduced by 5% H_2/He at room temperature (B). (From: rapid monitoring of the nature and interconversion of supported catalyst phases and of their influence upon performance: CO oxidation to CO_2 by γ-Al_2O_3 supported Rh catalysts in [33] Copyright Wiley–VCH Verlag GmbH & Co. KGaA. Reproduced with permission.)

3. Rhodium/alumina catalysts

Rhodium catalysts were prepared using a conventional method of impregnation of rhodium(III) chloride or nitrate onto a high area non-porous alumina (Degussa aluminium oxide C, area ~100 $m^2\ g^{-1}$) [32]. The choice of support was to minimize gas diffusion constraints. Following a drying and calcination stage, the samples were reduced by hydrogen. Samples were stored in closed vials in air. These catalysts mediated all three of the roles in a Three Way Catalyst (TWC) for automotive gas control, namely the removal of CO, NO and unburnt fuel (modelled here by H_2/He) [33].

The initial Rh K-edge x-ray absorption spectra recorded in either type of cell under helium indicated that these samples were all substantially oxidized (figure 1, spectrum A). Metallic materials could be readily regenerated under 5% H_2/He (figure 1, spectrum B). A pre-treatment cycle was employed of hydrogen reduction at 573 K under H_2 (until the partial pressure of H_2O was reduced to the baseline value), oxidation by 5% O_2/He (573 K until the CO_2 partial pressure attained a baseline level), and re-reduction by the H_2/He. This affords a common sample history for the supported metallic catalysts. Typically reaction gas mixtures were made either by mixing the diluted reagent gases in helium providing partial pressures in the 5–40 mbar range [28, 29, 33], or by switching between the 5% gas mixes in helium [32]. Such partial pressures are similar to, or higher than, those adopted in studies of automotive gas feeds (<10 mbar) [34]. For EXAFS analysis, the Debye Waller factors of the Rh–Rh first coordination shell were refined at each temperature on the same sample under a cooling cycle after heating to 623 K, this providing a more realistic estimate of this parameter to that derived from a metal foil [25].

3.1. Catalyst structure

Once prepared in the procedure described above, the 5 wt% Rh/Al_2O_3 catalysts exhibited reproducible x-ray absorption spectra displaying a XANES pattern which could be modelled with FEFF8.2 [35] by a fcc particle of ~43 atoms [19]. This is largely consistent with the first shell (2.67 Å) Rh–Rh coordination number of 7(±0.6) [20] refined by EXAFS analysis using EXCURV98 [36] considering the relationship between three-dimensional particle size and coordination number [21]. The EXAFS result represents a mean particle nuclearity rather than a specific cluster size. The first 2 non-nearest neighbour shells (3.776 and 4.65 Å) could also be located which indicates a three-dimensional morphology rather than a (111) raft [21]. A 2.5 wt% Rh/Al_2O_3 sample afforded a first shell coordination number of 6 when reduced at room temperature and 4.2 when reduced at 573 K [20]. XANES modelling indicates mean fcc cluster sizes of 19 and 10 atoms respectively [19].

3.2. Effect of reacting gases

Two oxidizing (O_2 and NO) and two reducing (H_2 and CO) gases, representative of present in automotive exhaust gases have been investigated, together with two sources of sulfur (H_2S and SO_2), a potential catalyst poison. It should be noted that the ability of CO to stabilize the $Rh^I(CO)_2$ centre [6] affords it an ambivalent role; generally in those cases surface hydroxyl groups are the oxidizing agents [37]. Even under hydrogen there is some apparent variation of coordination number with temperature when the 5 wt% Rh/Al_2O_3 catalyst is maintained at temperature under a flow of 5 wt% H_2/He [35], reducing from ~7 at ambient temperatures to ~4.5 at 573 K;

only some of this effect may be attributed to increasingly poor modelling of the atomic pair distributions by a simple Gaussian model at increasing temperature [22].

With most of the other gases the variations were more definitive, resulting in a change in the mean oxidation state of the rhodium. O_2 reacts exothermically at room temperature causing substantial changes in the Rh K-edge XAFS [33]; the Rh–Rh first coordination shell and the non-bonded shells are substantially reduced in intensity with a new component attributable to Rh–O (2.04 Å) evident. There is a substantial change in the XANES features, which can be modelled as a proportion of the rhodium in octahedral Rh_2O_3 type sites [19]. The change in XANES also provides a spectroscopic contrast which can be used to monitor this oxidation (and its reverse) kinetically [28]. However, the residual Rh···Rh shells do not match those expected for bulk Rh_2O_3, but are diminished versions of those in an fcc metal. Controlled oxidation of Rh(111) [39] and Rh(110) [40] surfaces has been shown to afford an O–Rh–O trilayer on the surface of the metal. This expands the unit cell and increases the first Rh–Rh distance by ∼0.35 Å. There are no new shells at this distance observed in the Rh EXAFS data on the supported metal particles, but the relatively low nuclearity of the particles involved, more like the Chini type of cluster $[Pt_{38}(CO)_{44}]^{2-}$ [41, 42], cannot provide such an extended overlayer to establish these repeating units. Rather there appears to be a rapid oxidation of the surface rhodium atoms, with a slower deeper oxidation which increases with time and temperature (up to 573 K) [28, 33] i.e. the Rh nanoparticles can be envisaged as a metal core with an oxidic outer layer (its thickness depending on the time and temperature of oxygen exposure).

Adsorption of NO is also a strongly exothermic process, and is accompanied by the evolution of N_2 and N_2O [43]; the resulting NO/Rh stoichiometry varies between 0.5 and 1.8 depending upon both the temperature and the metal loading [38]. There is a diversity of adsorption pathways which can be identified both by XAFS and IR spectroscopy. Starting from the smaller clusters (2 wt% Rh), at lower temperatures $Rh(NO)_2$ (υ(NO) = 1745 and 1835 cm^{-1}) and $Rh(NO^-)$ (υ(NO) = 1745 cm^{-1}) centres are dominant, with little N_2 being formed. As the temperature is raised above 373 K, a linear $Rh(NO^+)$ site with a higher υ(NO) stretching frequency (1910 cm^{-1}) becomes prevalent. On the higher loading sample, 5 wt% Rh, a fourth site is predominant at room temperature (υ(NO) = 1680 cm^{-1}) thought to be either a bent nitrosyl and/or NO on a metal surface. This too converts to the high frequency linear nitrosyl at elevated temperatures [38]. This site has been ascribed to a single rhodium atom on an oxidic site, the XANES pattern being modelled by a $[(-O)_3Rh(NO)]$ unit [29]. Correlations between the XANES, IR and mass spectrometry patterns have suggested that the bent nitrosyl (υ(NO) = 1745 cm^{-1}) is associated with N_2O formation up to 523 K, but there is a more apparent relationship with the appearance of the $[(-O)_3Rh(NO)]$ above that temperature [44].

The ability of oxide supported rhodium catalysts to afford $Rh(CO)_2$ centres has been known for over 50 years [45], but it was only by the application of XAFS spectroscopy that these could be assigned to oxidic sites with the metal in an overall Rh(I) oxidation state [9]. The rate of this reaction for a 2 wt% sample has been monitored by EDE over a period of 12 s [46] and within that time showed the loss of Rh–Rh bonds and the growth of backscattering Rh–O and Rh–CO units. This is considered to proceed via two intermediates: one with a terminal CO IR band (2060 cm^{-1}) due to binding on a metal cluster and the second monocarbonyl species occurs once a Rh–CO had migrated onto the oxide surface. Such an unsaturated intermediate might be similar to that generated photochemically from $Rh(CO)_2/Al_2O_3$ [47]; in that study the $(-O)_xRh(CO)$ species could not be observed, since it was reactive enough to cleave a C–H in cyclohexane. Similar studies under methane also identified a monocarbonyl species exhibiting an absorption at 2060 cm^{-1}, and this was now assigned to the M–CO unit in $[(-O)_xRh(H)(CO)\{C(O)CH_3\}]$ [48].

In our hands a 2.5 wt% Rh/Al_2O_3 sample did lose the Rh–Rh bonds on exposure to 5% CO/He for 50 s at room temperature and create a $Rh(CO)_2$ unit; the IR spectra however showed a further terminal band at ∼2060 cm^{-1} and a broad band due to bridging sites peaked at ∼1860 cm^{-1} [20]. The larger clusters in a 5 wt% sample showed only a small reduction in the Rh–Rh first coordination shell (from ∼6.9 to ∼6.6) on exposure to 5% CO/He up to 423 K. The IR spectra also demonstrated at the same time some $Rh(CO)_2$ formation, but with increased relative intensity of the terminal (2055 cm^{-1}) and bridging (1893 cm^{-1}) absorptions. These observations parallel well with HREELS and LEED studies of CO/Rh(111) [49], with the atop (terminal) site occurring at 2070 cm^{-1} at saturation coverage and a hollow site (μ_3-bridging) at 1861 cm^{-1}, rather than an edge (μ_2) site. $Rh(CO)_2$ species are not expected to be formed on a metal single crystal surface. The higher frequency bridging band (1893 cm^{-1}) observed for the 5 wt% Rh sample may be due to the occurrence of edge bridging sites for adsorbed CO.

The two sources of sulfur, a potential catalyst poison, both afforded exothermic adsorptions [50]. The larger gas uptake was observed for SO_2 (3.8/Rh). This was reflected only in the smaller reduction in Rh–Rh coordination number (from 7.0 to 5.7 after 5 min exposure to 5% SO_2/He at 300 K) whereas no Rh–O or Rh–S shells were being observed. Evidently the major interaction of SO_2 is with the surface of the alumina, probably forming surface sulfate (IV). In contrast, 5% H_2S/He caused an evolution of H_2, a rapid (<5 s) reduction in the Rh–Rh coordination number with an increase in mean Rh–Rh distance accompanied by the formation of a new Rh–S contribution (Rh–S 2.29 Å). A slower second stage process (50 s) followed by which point coordination numbers of 2 for both Rh–S and Rh–Rh contributions were observed, with an increase in Rh–Rh distance to 2.72 Å. Combining these structural features with the observed uptake of H_2 S (0.63S/Rh) and these structural features, the closest model for the new phase would be a sub-sulfide like $Rh_{17}S_{15}$ [51].

3.3. Relationship to catalyst performance

So CO, NO, O_2 and H_2 S all largely modify the rhodium nanoparticles by reducing the size of the metallic particles, and

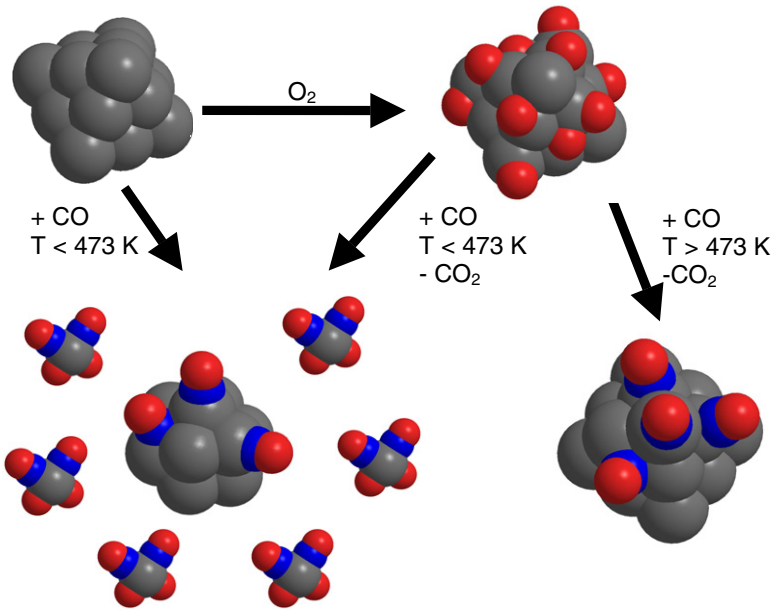

Figure 2. Representation of the structural changes of 5 wt% Rh/Al_2O_3 under conditions relating to CO oxidation by O_2 [33]. Rh atoms shown as larger spheres, carbon as dark, smaller and oxygen as light, smaller spheres.

affording either oxidic (O_2 and NO) or sulfidic (H_2S) regions or expelling single atoms stabilized by their adsorbates (CO and NO). Hence catalytic reactions involving these reagents may well also be accompanied by such structural changes. Three way exhaust catalysts show different efficiencies for removal of gases from the engine effluent. The NO_x removal is more efficient under reducing conditions, whereas the removal of CO and hydrocarbons is more efficient under lean-burn (oxidizing) conditions [52].

Under both CO rich and lean atmospheres 5 wt% Rh/Al_2O_3 was found to be an effective catalyst for CO oxidation [33]. However the temperature of the onset of activity (light-off) increased with the relative pressure of CO/O_2 and a different structural behaviour of the metal particles is observed and this is schematically represented in figure 2. At high CO ratios ($CO:O_2 > 2.5:1$), the particles start as partially oxidized but as the temperature was raised they became more reduced. The mean particle size increased (to ∼8.5) at high catalytic conversion (at temperatures above the light-off temperature). In CO lean conditions ($CO:O_2 = 0.11$; conversion 90% at 448 K) the Rh–Rh coordination decreased to ∼2.5, and the XANES features indicated a high degree of metal oxidation (70–80% at 448 K). Under a $CO:O_2$ mix of 2.5:1 there is lower catalytic activity at this temperature (40% conversion). The XAFS analysis showed that ∼40% of the rhodium was sequestered as $Rh(CO)_2$ centres and the remaining rhodium is in a metallic form with CO adsorbed. At 473 K (conversion 80%) the $Rh(CO)_2$ centres decomposed and the metallic particles reformed. Activity appears to be correlated with surfaces incompletely covered with CO and which are partially oxidized thus providing adsorption sites for both reagents and migration pathways on the surface (figure 2).

In contrast there is no significant catalytic activity for the reduction of NO by H_2 under oxidizing conditions [32]; activity is evident and sustained only when the rhodium is present as metallic particles i.e. at H_2/NO ratios of >1. Not surprisingly, in view of their different forms of interaction with the Rh/Al_2O_3, SO_2, which interacts with the oxide surface does not poison NO reduction, but H_2S, which converts the metallic particles to a sulfide, arrests the activity when pulsed into a working catalyst at 525 K [50].

When exposed to a 1:1 mixture of 5% NO/He and 5% CO/He, the 5 wt% Rh/Al_2O_3 catalyst is rapidly partially oxidized with the Rh–Rh first shell coordination number reducing to ∼3 at ambient temperature [14]. The changes in IR intensity, coordination number and NO concentration are shown in figure 3. The Rh–Rh coordination number is further reduced on raising the temperature to 450 K, with a simultaneous increase in the intensity of the IR bands of the $Rh(CO)_2$ units. Evidently, the presence of NO enhances the formation of these mononuclear Rh^I sites as carbonyls. Above 450 K the $Rh(CO)_2$ units begin to decompose and Rh aggregation ensues; it is at this point that the reduction of NO by CO becomes evident. At even higher temperatures (573 K for a catalyst with $RhCl_3$ as the metal source), the particle size increases again, with the $Rh(CO)_2$ now absent, and the principal IR absorption is observed at ∼1910 cm^{-1}, due to the (O_x–Rh–NO) site [53]. By carrying out pulsed gas switching experiments (here, every 10 s) between 5% NO/He and 5% CO/He, one can identify different types of structural changes below and above the light-off temperature [29]. Below the light-off temperature (473 K), the gas switch primarily causes an interconversion between the two oxidic sites: $Rh(CO)_2$ and O_x–Rh–NO, as shown by the IR spectra in figure 4. The mean Rh–Rh coordination number hovered near a value of 4. However at 623 K the mean first shell occupancy varies between 8 with a CO pulse, and 5 on introduction of NO. The changes in coordination number, IR intensities and

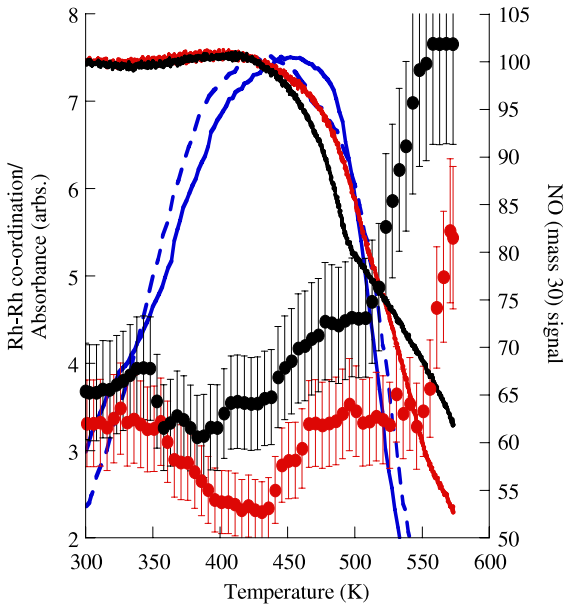

Figure 3. Variation in Rh–Rh coordination (filled circles), net NO signal (—), during NO reduction by CO over chlorinated (lighter) and non-chlorinated (black) Rh/Al_2O_3 catalysts. The intensity of the asymmetric stretch of the $Rh^I(CO)_2$ species (dashed for the chlorinated case) is also shown. (From: synchronous, time-resolved, diffuse reflectance FT-IR, energy dispersive EXAFS (EDE) and mass spectrometric investigation of the behaviour of Rh catalysts during NO reduction by CO in [14] Copyright Royal Society of Chemistry Reproduced with permission.)

mass spectrum responses during the switching experiments are presented in figure 4. The CO sites adopted are the atop and bridging sites typical for a metal particle, and these are replaced by the (O_x–Rh–NO) site after the NO switch. As the gas switch occurs, the two monoxides react to form N_2, N_2O and CO_2, with the faster reaction being between NO and Rh-bound CO, rather than the obverse reaction. A schematic representation of the of the structural changes under NO and CO is presented in figure 5.

3.4. Modifying the rhodium catalyst

The energy bandwidth on ID24 with a Si(111) monochromator allows coverage of both the Rh and Pd K-edges simultaneously, thus the structural changes at each of two of the common transition metal components of the three way catalyst can be monitored in parallel [54]. Interestingly, the substitution of 1/5 of the rhodium by palladium ($4\%Rh–1\%Pd/Al_2O_3$) provides protection for the rhodium from oxidation under a 3:2 NO–H_2 reagent mix; up to 600 K the Rh–Rh/Pd coordination number remains between 9 and 10. Viewed from the Pd edge, the metal–metal coordination number is ∼6 at room temperature, suggesting some surface segregation. This value rises to ∼9.5 at the light-off temperature, which is 60 K lower on addition of palladium. Evidently the distribution of the metals within the alloy particles changes under these reaction conditions.

A higher RhPd particle size (Rh–Rh/Pd coordination number 6–6.5) is observed for the $4\%Rh–1\%Pd/Al_2O_3$ catalyst used under NO/CO (1:1) compared to the Rh only system, but to a much lower extent than under NO/H_2 [53]. Some $Rh(CO)_2$ centres are evident by IR up to 500 K, so these Rh atoms will have been removed from the alloyed particles. The residual alloyed clusters may have a nuclearity of ∼20 atoms, with palladium atoms at capping positions retarding further fragmentation; indeed in a 19 atom octahedron with this arrangement would mean that all surface rhodium atoms would also be bonded to palladium atoms [53]. In this system, the presence of the palladium slightly increases the light-off temperature but the selectivity N_2/N_2O is extremely similar to the rhodium only catalyst, implying that metallic rhodium sites are key for this reaction.

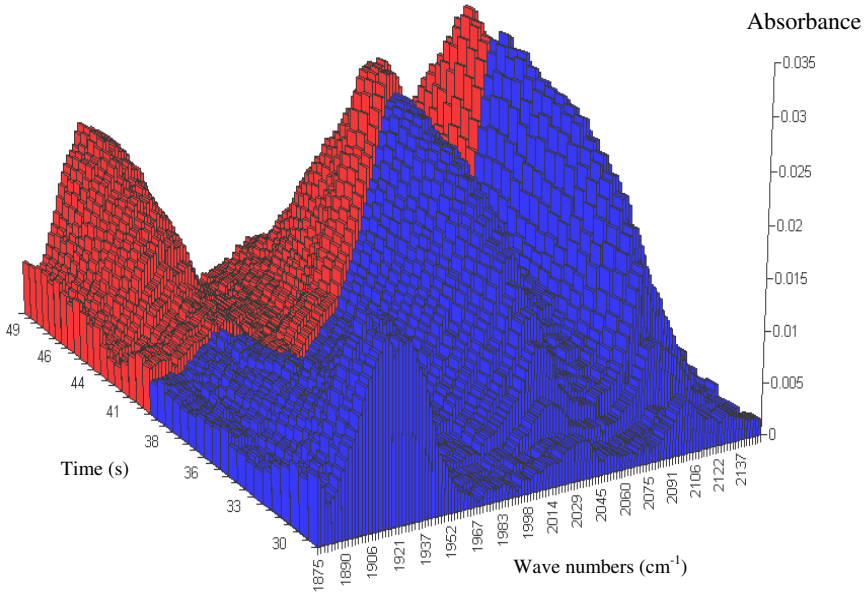

Figure 4. Variations in the IR spectra observed from 5 wt% Rh/Al_2O_3 during switches between 5% NO/He 5% CO/He at 473 K. Switch from NO to CO at 30 s and back to NO at 40 s. (From: rhodium dispersion during NO/CO conversions in [29] copyright Wiley–VCH Verlag GmbH & Co. KGaA. Reproduced with permission.)

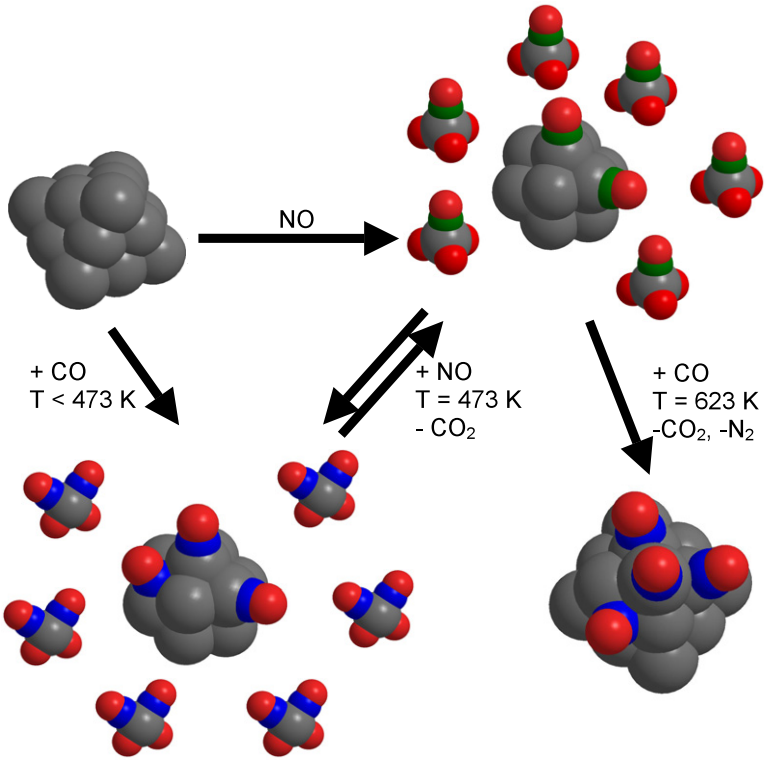

Figure 5. Representation of the structural changes of 5 wt% Rh/Al_2O_3 under conditions relating to CO oxidation by NO [29]. Rh atoms shown as larger spheres, carbon as dark, smaller, nitrogen as medium-grey smaller and oxygen as light grey, smaller spheres.

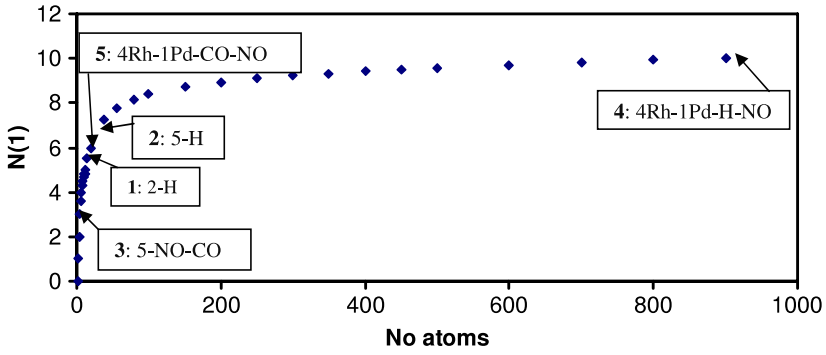

Figure 6. Plot of first shell coordination numbers versus particle nuclearities based on [21]. Points are indicted for **1**: 2-H: 2.5% Rh/Al_2O_3 reduced, 5%H_2/He, room temperature; **2**: 5-H 5% Rh/Al_2O_3 reduced, 5%H_2/He, room temperature; **3**: 5-H: 5% Rh/Al_2O_3 under 2.5%NO–2.5%CO/He (300–550 K); **4** 4Rh–1Pd–H–NO: 4%Rh–1%Pd/Al_2O_3, under 3%NO–2%H_2/He; **5**: 4Rh–1Pd–CO–NO: 4%Rh–1%Pd/Al_2O_3, under 2.5%NO–2.5%CO/He.

4. Concluding comments

In this report, we observe mean nuclearities of up to 1000 atoms, so these functional materials span the classes of metal clusters and nanoparticles. The three catalyst materials described, each have substantially different particle sizes after reduction under H_2/He (figure 6), increasing from ∼19 atoms for the 2.5 wt% Rh/Al_2O_3 (at room temperature), through ∼40 for the 5 wt% Rh/Al_2O_3 to ∼1000 for 4%Rh–1% Pd/Al_2O_3. Additionally these materials exhibit very different particle sizes under different gas mixtures, even for these examples which vary relatively little with temperature (figure 6). The most marked change is that for the alloy catalyst dropping down to mean nuclearity of ∼19 metal atoms under CO/NO. In other environments, as for Rh/Al_2O_3 under NO/CO, NO/H_2 and O_2/CO, within the temperature range studied there is a substantial change in the mean oxidation state of the rhodium accompanied with a mean nuclearity change. In the presence of strongly coordinating reagents like CO and NO, oxidized centres can be stabilized as mononuclear sites, with the nitrosyl providing the more thermally robust centre. Oxidants like O_2 and H_2S without the steric block afforded by a linear diatomic ligand, instead provide small partially oxidized metal–chalcogenide clusters.

It appears that metallic clusters are required for the dissociative steps in the reactions of NO and O_2, and these

are not provided by the mononuclear centres, which are likely to act as spectator species. The different mono-and multi-nuclear species are in a dynamic equilibrium which at ∼573 K is established within seconds. The dynamic changes might in the worst case sequester some of the metal in relatively inactive forms. On the other hand this dynamic behaviour may well be the secret to success for catalysts to respond to rapidly changing conditions, such as those in an engine management system. Catalyst longevity may be ascribed to a high degree of and rate of chemical reversibility rather than being due to a monolithic unchanging catalyst particle.

Trying to gain an atomic level understanding of these processes is challenging both for characterization techniques and in experimental design. Part of the story can be revealed by imaging studies on single crystal surfaces, but a more complete description requires such phases to be registered on supports of known surface structure, such as studies of single crystal oxide surface [55, 56]. However, even in those circumstances, the adlayers may not register in an ordered manner [56].

Acknowledgments

We wish to thank the Directors of the ESRF for access to their facility, and to the staff on ID24 for their invaluable assistance. We also wish to thank EPSRC for support through research grants (GR/L13841, R/60744, S/85818) and for an Advanced Fellowship (EP/E060404 to MT). The research is also part of the ICECAT Network of Excellence (NMP-CT-2005-011730).

References

[1] Berzelius J 1836 *Jahres-Bericht über die Fortschritte der Physichem Wissenschaften* vol 15 (Tübingen: H Laupp)
[2] Somorjai G A 1994 *Introduction to Surface Chemistry and Catalysis* (New York: Wiley)
[3] Ertl G 2002 *J. Mol. Catal.* A **182/183** 5
[4] Knözinger H 1988 *Surface Organometallic Chemistry: Molecular Approaches to Catalysis NATO ASI Ser.* 231 ed J-M Basset, B C Gates, J-P Candy, A Choplin, M Leconte, F Quignard and C Santini (Dordrecht: Kluwer) p 35
[5] Basset J-M, Gates B C, Candy J-P, Choplin A, Leconte M, Quignard F and Santini C (ed) 1988 *Surface Organometallic Chemistry: Molecular Approaches to Catalysis NATO ASI Ser.* 231 (Dordrecht: Kluwer)
[6] Che M and Bennett C O 1989 *Adv. Catal.* **36** 55
[7] Evans J 1981 *Chem. Soc. Rev.* **10** 159
[8] Lytle F W, Greegor R B, Marques E C, Sandstrom D R, Via G H and Sinfelt J H 1985 *J. Catal.* **95** 546
[9] van't Blik H F J, van Zon J B A D, Huizinga T, Vis J C, Koningsberger D C and Prins R 1985 *J. Am. Chem. Soc.* **107** 3139
[10] Briois V, Lützenkirchen-Hecht D, Villain F, Fonda E, Belin S, Griesebock B and Frahm R 2005 *J. Phys. Chem.* A **109** 320
[11] Matsushita T and Phizackerley R P 1981 *Japan. J. Appl. Phys.* **20** 2223
[12] Evans J 1997 *Chem. Soc. Rev.* **26** 11
[13] Newton M A, Dent A J and Evans J 2002 *Chem. Soc. Rev.* **31** 83
[14] Newton M A, Jyoti B, Dent A J, Fiddy S G and Evans J 2004 *Chem. Commun.* 2382
[15] Beale A M, van der Eerden A M J, Kervinen K, Newton M A and Weckhuysen B M 2005 *Chem. Commun.* 3015
[16] Tromp M *et al* 2007 *AIP Conf. Proc.* **882** 858
[17] Tromp M, Sietsma J R A, van Bokhoven J A, van Strijdonck G P F, van Haaren R J, van der Eerden A M J, van Leeuwen P W N M and Koningsberger D C 2003 *Chem. Commun.* 128
[18] Dent A J, Wells M P, Farrow R C, Ramsdale C A, Derbyshire G E, Greaves G N and Thomas J M 1992 *Rev. Sci. Instrum.* **63** 903
[19] Tromp M 2006 unpublished results in [20]
[20] Jyoti B 2006 *PhD Thesis* University of Southampton
[21] Jentys A 1999 *Phys. Chem. Chem. Phys.* **1** 4059
[22] Koningsberger D C and Prins R (ed) 1988 *X-ray Absorption Spectroscopy* (New York: Wiley)
[23] Frenkel A I 1999 *J. Synchrotron Radiat.* **6** 293
[24] Greegor R B and Lytle F W 1980 *J. Catal.* **63** 476
[25] Clausen B S and Nørskov J K 2000 *Top. Catal.* **10** 221
[26] Fiddy S G, Newton M A, Dent A J, Salvini G, Corker J M, Turin S, Campbell T and Evans J 1999 *Chem. Commun.* 851
[27] Fiddy S G, Newton M A, Campbell T, Dent A J, Harvey I, Salvini G, Turin S and Evans J 2002 *Phys. Chem. Chem. Phys.* **4** 827
[28] Newton M A, Fiddy S G, Guilera G, Jyoti B and Evans J 2005 *Chem. Commun.* 118
[29] Dent A J, Evans J, Fiddy S G, Jyoti B, Newton M A and Tromp M 2007 *Angew. Chem. Int. Edn* **46** 5356
[30] Newton M A, Burnaby D G, Dent A J, Diaz-Moreno S, Evans J, Fiddy S G, Neisius T, Pascarelli S and Turin S 2001 *J. Phys. Chem.* A **105** 5965
[31] Bravin A, Fiedler S, Coan P, Labiche J C, Ponchut C, Peterzol A and Thomlinson W 2003 *Nucl. Instrum. Methods Phys. Res.* A **510** 35
[32] Newton M A, Dent A J, Diaz-Moreno S, Fiddy S G and Evans J 2002 *Angew. Chem. Int. Edn* **41** 2587
[33] Newton M A, Dent A J, Diaz-Moreno S, Fiddy S G, Jyoti B and Evans J 2006 *Chem. Eur. J* **12** 1975
[34] Harmsen J M A, Hoebink J H B J and Schouten J C 2001 *Catal. Lett.* **71** 81
[35] Ankudinov A L, Bouldin C, Rehr J J, Sims J and Hung H 2002 *Phys. Rev.* B **65** 104107
[36] Binsted N 1998 *EXCURVE98* CCLRC Daresbury Laboratory program
[37] Paul D K, Marten C D and Yates J T 1999 *Langmuir* **15** 4508
[38] Newton M A, Dent A J, Fiddy S G, Jyoti B and Evans J 2007 *J. Mater. Sci.* **42** 3288
[39] Gustafson J, Mikkelsen A, Borg M, Lundgren E, Köhler L, Kresse G, Schmid M, Varga P, Yuhura J, Torrelles X, Quirós C and Andersen J N 2004 *Phys. Rev. Lett.* **92** 126101
[40] Gustafson J, Mikkelsen A, Borg M, Anderson J N, Lundgren E, Klein C, Hofer W, Schmid M, Varga P, Köhler L, Kresse G, Kasper N, Stierle A and Dosch H 2005 *Phys. Rev.* B **71** 115442
[41] Chini P 1980 *J. Organomet. Chem.* **200** 37
[42] Ceriotti A, Masciocchi N, Macchi P and Longoni G 1999 *Angew. Chem. Int. Edn* **38** 3724
[43] Campbell T, Dent A J, Diaz-Moreno S, Evans J, Fiddy S G, Newton M A and Turin S 2002 *Chem. Commun.* 304
[44] Newton M A, Dent A J, Fiddy S G, Jyoti B and Evans J 2007 *Phys. Chem. Chem. Phys.* **9** 246
[45] Yang A C and Garland C W 1957 *J. Phys. Chem.* **61** 1504
[46] Suzuki A, Inada Y, Yamaguchi A, Chihara T, Yuasa M, Nomura M and Iwasawa Y 2003 *Angew. Chem. Int. Edn* **42** 4795
[47] Wong J C S and Yates J T 1994 *J. Am. Chem. Soc.* **116** 1610

[48] Wong J C S and Yates J T 1995 *J. Phys. Chem.* **99** 12640
[49] Linke R, Curulla D, Hopstaken M J P and Niemantsverdriet J W 2001 *J. Chem. Phys.* **115** 8209
[50] Newton M A, Dent A J, Diaz-Moreno S, Fiddy S G, Jyoti B and Evans J 2003 *Chem. Commun.* 1906
[51] Parthe E, Hohnke D and Hulliger F 1967 *Acta Crystallogr.* **23** 832
[52] Twigg M V 2006 *Catal. Today* **117** 407
[53] Tromp M, Dent A J, Evans J, Fiddy S G, Jyoti B and Newton M A 2008 *Discuss. Faraday Soc.* **138** at press doi:10.1039/b706294j
[54] Newton M A, Jyoti B, Dent A J, Diaz-Moreno S, Fiddy S G and Evans J 2004 *ChemPhysChem* **5** 1056
[55] Evans J, Hayden B, Mosselmans F and Murray A 1994 *Surf. Sci.* **301** 61
[56] Bennett R A, Newton M A, Smith R D, Bowker M and Evans J 2001 *Surf. Sci.* **487** 223